



## Zinc oxide nanoparticles: An experimental study of synthesis, characterization and biological activity

AULA M. AL HINDAWI<sup>1</sup>, ZAHRAA M. ABD AL-AAMA<sup>1</sup>, JUMAN KHALEEL AL-SABBAGH<sup>2</sup> and MOHAMMED AWAD<sup>3,4\*</sup>

<sup>1</sup>Department of Chemistry, College of Education for Pure Science, University of Kerbala, Karbala, Iraq, <sup>2</sup>College of Veterinary Medicine, University of Kerbala, Karbala, Iraq,

<sup>3</sup>School of Engineering, Samarkand International University of Technology, Samarkand, Uzbekistan and <sup>4</sup>Department of Chemical Engineering, Toronto Metropolitan University, Toronto, Canada

(Received 19 March, revised 22 April, accepted 24 August 2024)

**Abstract:** Zinc oxide (ZnO) nanosized structures were synthesized successfully using a benign method. The latter can be achieved by introducing sesame seed extract into the formation process of ZnO nanostructures as a reducing agent, converting zinc ions to Zn. The structural and optical properties of the prepared ZnO particles were studied using many techniques such as UV–Vis spectrophotometry, field emission scanning electron microscopy (FE-SEM), energy-dispersive X-ray spectroscopy (EDS), X-ray diffraction (XRD) and Fourier-transform infrared spectroscopy (FTIR). The estimated band gap energy of ZnO nanoparticles formed in the presence and absence of extract was found to be 3.94 and 3.88 eV, respectively, suggesting the effect of quantum confinement. The prepared particles have a flower-like shape with the appearance of small spherical particles. A Tauc plot was utilized to estimate the band gap energy of ZnO nanoparticles. The findings show that ZnO nanoparticles display bactericidal properties against *Staphylococcus hominis*, which are Gram-positive bacteria, and also on Gram-negative bacteria such as *Proteus mirabilis*, *E. coli*, *Acinetobacter baumannii*, *Pseudomonas aeruginosa* and *Klebsiella pneumonia*.

**Keywords:** ZnO-NPs; antibacterial activity; sesame seeds.

### INTRODUCTION

Bacteria are known to be the cause of many infectious illnesses. The treatment of such diseases has become challenging due to their resistance to antibiotics.<sup>1,2</sup> To protect human society, new medications or techniques for killing these micro-organisms must be developed. Nanotechnology is a developing area where the

\* Corresponding author. E-mail: E-mail: mohammed.awad@torontomu.ca;  
mohammed.awad@siut.uz  
<https://doi.org/10.2298/JSC240319079A>

nanostructures of varying shapes and sizes can be manufactured, offering potential applications as antibiotics.<sup>3</sup> Because of their tiny size at the nanoscale, the nanostructures can infiltrate bacteria cell walls and engage with the cell membrane subsequent to adhering to the cell wall.<sup>3</sup> Unlike their larger counterparts, these particles possess expansive surface areas, amplifying their reactivity and potential toxicity. Many metal oxide nanoparticles are incredibly damaging to certain types of bacteria. For example, titanium dioxide ( $\text{TiO}_2$ ) nanoparticles can eliminate *Escherichia coli* bacteria.<sup>4</sup> Likewise, the nanoparticles of magnesium oxide ( $\text{MgO}$ ) and calcium oxide ( $\text{CaO}$ ) show the bactericidal effects against *Bacillus cereus*, *Bacillus globigii* and *E. coli*.<sup>5,6</sup>

Zinc oxide ( $\text{ZnO}$ ) nanoparticles (NPs) are highly regarded as effective photocatalysts and antimicrobial agents because they can generate free radicals.<sup>7</sup> When  $\text{ZnO}$  particles encounter the solar radiation exceeding their band gap energy, electrons become energized to the conduction band (CB), leaving vacancies known as holes in the valence band (VB).<sup>8</sup> The photogenerated electrons and holes generated on the surface of  $\text{ZnO}$  lead to the creation of highly reactive oxygen species (ROS), like superoxide anion ( $\bullet\text{O}_2$ ) and hydroxyl radical ( $\bullet\text{OH}$ ). These extremely reactive oxygen species perform antibacterial and photodegradative activities by destroying bacteria's DNA and membrane. Moreover, studies show that Zn ion could damage the bacteria's cell membrane, changing the metabolic pathway. Yang *et al.* showed that the antibacterial effectiveness of  $\text{ZnO}$ -NPs at concentrations of 10 and 50 mg L<sup>-1</sup> were 28.30 and 55.03 %, respectively. Their findings showed that increasing the concentration of  $\text{ZnO}$ -NPs increases the antibacterial effect due to their small size and high specific surface area.<sup>9</sup> This antibacterial activity of  $\text{ZnO}$ -NPs paves the way for use in many potential fields, such as in producing UV-blocking clothing, sunscreens, infant rash ointments, paints, drug delivery and even food preservatives.<sup>10–12</sup>

$\text{ZnO}$ -NPs can be produced using various techniques, including co-precipitation,<sup>13</sup> sol-gel,<sup>14,15</sup> hydrothermal<sup>16</sup> and solochemical.<sup>7</sup> The size, shape, surface area, electronic states and surface charge of nanostructures majorly impact their biological activities. Therefore, the synthesis process must be chosen to produce nanosized materials with the best activity for the intended applications. This work is aimed to present a method to fabricate  $\text{ZnO}$  nanostructures using an eco-friendly and straightforward green method and chemical precipitation method. Their bacterial activity is examined against Gram-positive bacteria (*Staphylococcus hominis*) and Gram-negative bacteria (*Proteus mirabilis*, *E. coli*, *Acinetobacter baumannii*, *Pseudomonas aeruginosa* and *Klebsiella pneumonia*). The basic idea behind this green synthesis is to use parts of plants such as seeds, leaves, and roots as reducing and stabilizing agents instead of chemical solvents and agents. The green synthesized  $\text{ZnO}$ -NPs were considered safe for pharmaceutical and biomedical applications.<sup>17</sup>

## MATERIALS AND METHODS

### Materials

In this project, zinc sulfate heptahydrate ( $\text{ZnSO}_4 \cdot 7\text{H}_2\text{O}$ , 99 %) was purchased from Thomas Baker. Scharlau supplied sodium hydroxide ( $\text{NaOH}$ , 99 %).

### Preparation of sesame seed solution

The sesame seeds were purchased from the local market and crashed into tiny fragments. Five grams of sesame seeds were dissolved in de-ionized water (100 mL). A magnetic stirrer (set at 150 rpm) was used to stir the solution for a few minutes at 60 °C. After that, filter paper No. 1 was used to achieve filtration, and the filtrate was refrigerated (4 °C) before being used to prepare zinc oxide nanoparticles.

### Preparation of $\text{ZnO-NPs}$

One mM of  $\text{ZnSO}_4 \cdot 7\text{H}_2\text{O}$  was prepared and stirred for 60 min at 25 °C. After adding 50 mL of the sesame seed extract to the precursor solution, the latter was stirred for 10 min. Subsequently,  $\text{NaOH}$  (1 M) was gradually added until the pH of the solution reached 10 while maintaining 70 °C and stirring. A yellowish-white precipitate was observed at the bottom of the mixture flask, suggesting the formation of  $\text{ZnO}$  (capped-ZnO-NPs). The centrifuge was used to collect the residue, which was formed, for 20 min at 4000 rpm. Ultimately, the final product underwent 4 h of vacuum oven drying at 80 °C after being repeatedly cleaned with distilled water. A similar procedure was performed to form the uncapped-ZnO nanoparticles without the addition of the sesame seed extract.

### Characterization techniques

Various characterization approaches were used to investigate the physicochemical properties of synthesized  $\text{ZnO}$ . UV-1800 Shimadzu spectrophotometer (Japan) was used to study the optical properties of zinc oxide nanostructures. The functional groups of the sesame seed extract were identified using the Fourier-transform infrared spectrum (FT-IR, Shimadzu). Using  $\text{CuK}\alpha$  radiation ( $\lambda = 0.154056$  nm) and a scanning range of 20 to 80°, the X-ray diffraction (XRD) patterns were recorded.

### Biological activity of $\text{ZnO-NPs}$

Various strains of bacteria sourced from different medical cases, including skin infections, urinary tract infections, genital infections, tonsillitis and ear infections, were tested. These bacteria were identified through biochemical methods and VITEK2 analysis.

$\text{ZnO-NPs}$  were prepared by dissolving 10 mg of  $\text{ZnO}$  powder in 100 mL distilled water. A pure culture of a bacterial organism that has been previously described (107 CFU) was used for the test. The inoculum was prepared by transferring five isolated colonies cultured on blood agar plates into 5 mL broth. This mixture was then incubated for 120 min to generate a moderately cloudy bacterial suspension. To acquire an inoculum from the standardized culture, a sterile swab was used and then transferred onto a Müller–Hinton plate to dry.

Next, the diffusion test (Kirby–Bauer susceptibility test) was used to determine the bacterial sensitivity to antibacterial agents. After inoculating the medium agar with the bacterial isolates, pores are created on agar plates using a poorer cork before drying the plates. The solution of  $\text{ZnO}$  was added into the pores and incubated overnight (37 °C). A caliper was used to measure the inhibitory zones. According to the standard zones from the Clinical and Laboratory Standard Institute (CLSI), the organism's resistance was identified.<sup>18</sup>

## RESULTS AND DISCUSSION

In Fig 1a, the appearance of the blue shift in the UV–Vis spectra of capped and uncapped-ZnO concerning their counterpart bulk (373 nm)<sup>19</sup> confirms the formation of ZnO at nanoscale levels. A large shift was observed when the sesame extract was introduced (capped-ZnO). A possible explanation for this shift is that adding the sesame extract prevents the further addition of atoms to the already existing particles. To estimate the energy of the band gap for the prepared ZnO-NPs, Tauc plot was used:<sup>20,21</sup>

$$\alpha h\nu = C(h\nu - E_g)^n \quad (1)$$

Herein, the band gap energy is  $E_g$ , the coefficient of absorption represented by  $\alpha$ . The  $n$  indicates a direct electronic transition and equals 0.5, which denotes Tauc exponent,<sup>22</sup> the proportional constant is  $C$  and the energy photon is  $h\nu$ .

Extending the linear portion of the UV–Vis spectrum along the photon energy axis in Fig. 1b, the band gap energy is determined to be 3.94 and 3.88 eV for capped and uncapped-ZnO, respectively. This value exceeds bulk ZnO (3.37 eV)<sup>23</sup> due to elections confinement at the nanoscale.<sup>24</sup> The band gap energy value closely aligns with findings from prior experiments, conducted by Miri *et al.*<sup>22</sup>

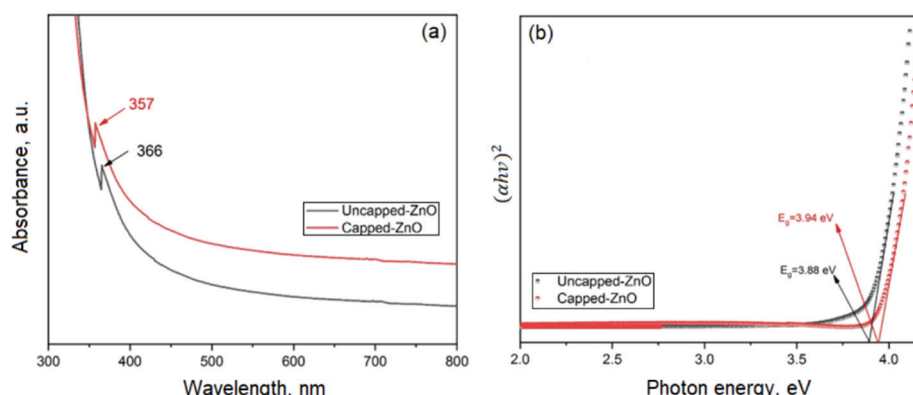


Fig. 1. a) UV–Vis spectrum of zinc oxide nanostructures formed in the presence of sesame seeds and b) the Tauc plot used to calculate the band gap ( $E_g$ ), which equals 3.94 eV.

The field emission scanning electron microscopy (FE-SEM) examined the surface morphology of both capped and uncapped-ZnO nanostructures. Fig. 2a shows that introducing sesame seeds into the synthesis process of ZnO particles has no effect on the morphology of the prepared samples. Both methods give particles with flower-like shapes in addition to the appearance of small spherical particles. The energy-dispersive X-ray spectroscopy (EDS) was used to study the elements that could be present in the sample. The energy dispersive X-ray analysis (EDX) chart for capped-ZnO in Fig. 2c (uncapped-ZnO nanoparticles not shown

in Fig. 2c as the chart is similar to capped-ZnO) in Fig. 2b shows that the sample contains zinc and oxygen elements in its structure, confirming the formation of ZnO nanostructures. The appearance of the gold component in the chart is attributed to the coating process for the semiconductor to make the sample conductor.<sup>25</sup>

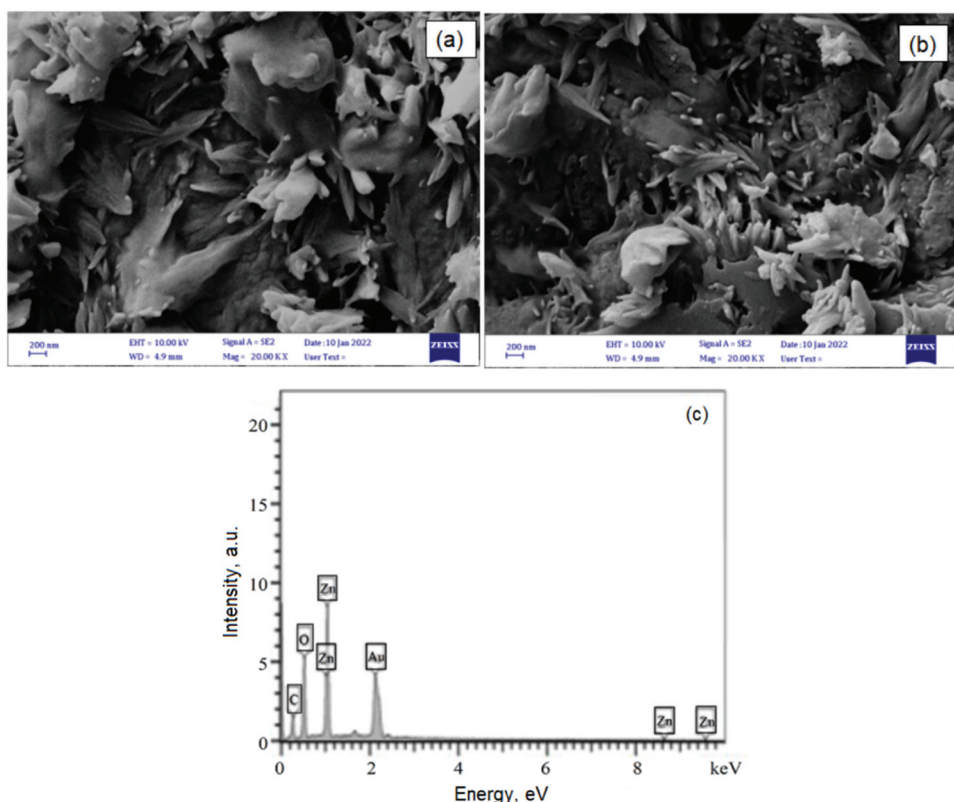


Fig. 2. a) The field emission scanning electron microscopy (FE-SEM) image of the prepared zinc oxide nanostructures in the presence of sesame seeds extract, b) FE-SEM image for uncapped-ZnO nanostructures and c) the energy dispersive X-ray analysis (EDX) chart showing the element in the capped-zinc oxide nanostructures sample.

The crystalline structure of the synthesized ZnO-NPs was examined using XRD. It is clear from Fig. 3 that the diffraction peaks appear at 30.03, 37.878, 48.21, 56.20, 63.69 and 67.24° correspond to 100, 002, 101, 102, 110 and 103 planes, respectively. This finding suggests that the as-prepared ZnO has a hexagonal wurtzite structure, which aligns with the previous studies.<sup>26,27</sup> The crystallite size was calculated for the highest intensity peak of 100 using Scherrer formula,<sup>28,29</sup> and it was found to be 20.2 nm. The interesting point here is that there was no effect seen at all on the crystalline properties of ZnO nanostructures

after introducing sesame seeds extract. Our speculation for this observation is that the bioactive components in the extract are attached to ZnO surface and form weak van der Waals forces, without any effect on the crystalline structures of ZnO.

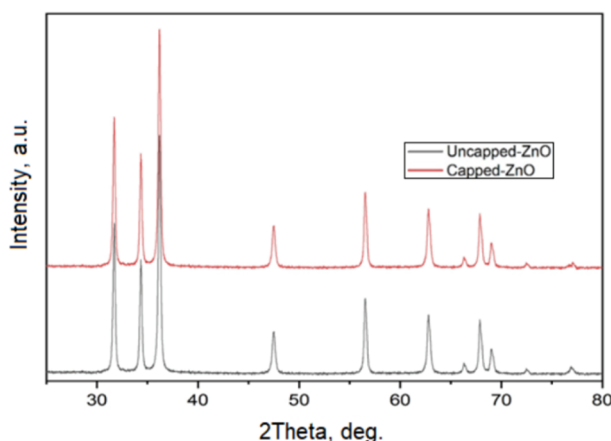


Fig. 3. X-ray diffraction (XRD) pattern for zinc oxide nanostructures prepared with sesame seed.

FTIR spectra for capped- and uncapped-ZnO nanostructures were measured between 500 and 4000  $\text{cm}^{-1}$ . In both samples, the peak centered at 558  $\text{cm}^{-1}$  is assigned to Zn–O vibration mode,<sup>30</sup> confirming the formation of ZnO-NPs (see Fig. 4). The spectrum of sesame seeds capped-ZnO exhibits several additional peaks which probably relates to the presence of bioactive constituents extracted from sesame seeds. For example, the peak appeared at 3340  $\text{cm}^{-1}$  could be related to the presence of the OH group from the alkaloid compound on the ZnO surface, while the absorption band at ~2950  $\text{cm}^{-1}$  corresponds to the C–H group.<sup>31,32</sup> The two peaks at 1527 and 1653  $\text{cm}^{-1}$  is ascribed to N–H binding and C–O, respectively, which represent the sugars existed within ZnO nanostructures. A strong peak centered at ~880  $\text{cm}^{-1}$  is assigned to (RCOOH), which is possibly related to phenolic compounds. The emergence of these peaks is ascribed to the presence of bioactive constituents extracted from sesame seeds. These components serve as reducing agents by supplying electrons, thereby facilitating the reduction of  $\text{Zn}^{2+}$  to  $\text{Zn}^+$  and subsequently to Zn (Zn nanoparticles).<sup>33</sup>

The antibacterial activity of prepared ZnO-NPs against different bacteria types was determined using a diffusion test for both capped, uncapped-ZnO nanoparticles and Zn ions alone. The appearance of clear zones on the Petri dishes indicates the ability of ZnO-NPs to inhibit the under-studying bacterial growth. The results found that uncapped ZnO-NPs had less effect as comparing to the capped ZnO-NPs with the sesame seeds extract; while Zn ions appear with no effect at all (Table I). Fig. 5a shows the antibiotic effect of ZnO nanocrystals against *Pseudo-*

*monads aeruginosa* (upper part), *Klebsiella pneumonia* (lower part) and Fig. 5b *E. coli* bacteria.

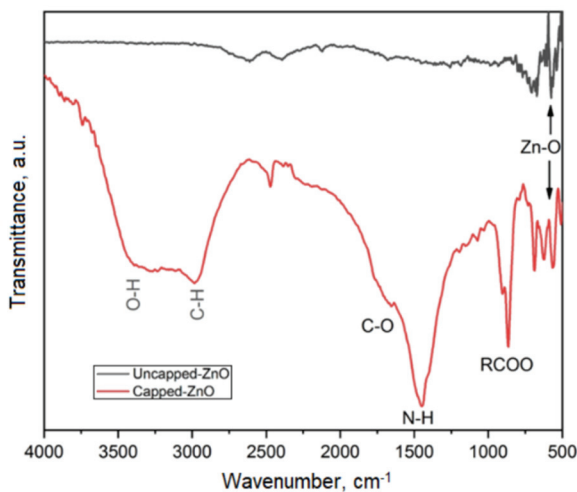


Fig. 4. Fourier-transform infrared spectroscopy (FTIR) for zinc oxide nanostructures.

TABLE I. The antibacterial effect of Zinc oxide nanoparticles (ZnO-NPs) was determined from the inhibition zones

No.	Bacterial isolates	Inhibition zone, mm
1	<i>Proteus mirabilis</i>	15
2	<i>Escherichia coli</i>	28
3	<i>Staphylococcus hominis</i>	22
4	<i>Acinetobacter baumannii</i>	18
5	<i>Pseudomonas aeruginosa</i>	25
6	<i>Klebsiella pneumoniae</i>	20

The rest of the chosen bacteria in this study and their inhibition zones, which formed around the particles, were calculated and presented in Table I. *E. coli* is more sensitive to the ZnO nanoparticles based on its inhibition zone (28 mm). It was known that the larger the inhibitory zone, the greater the sensitivity to the ZnO particles. According to a previous Klink *et al.*<sup>34</sup> study, the inhibition zone should be  $\geq 10$  mm for effectiveness. Although *P. mirabilis* shows a smaller inhibition zone (15 mm) than other strains, it is still considered adequate.

The best explanation for the antibiotic effect is that the small ZnO particles result in a high surface-to-volume ratio and more adherence to the Gram-positive and harmful bacteria. Several mechanisms for the antibacterial action of ZnO-NPs have been proposed. A possible mechanism is the adsorption of ZnO-NPs on the bacterial surface, which leads to product various intermediates and electrostatic interactions.<sup>35</sup>

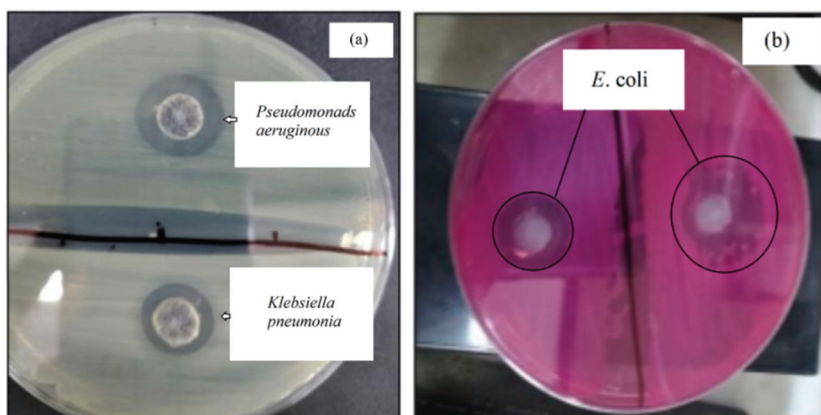


Fig. 5. The inhibition zones of zinc oxide nanoparticles against bacterial isolates:  
 a) *Pseudomonas aeruginosa* (upper part) and *Klebsiella pneumonia* (lower part) bacteria;  
 b) *Escherichia coli* bacteria.

On the other hand, Mendes *et al.*<sup>17</sup> have recently studied the membrane integrity of *P.s aeruginosa*, *E. coli*, *S. aureus* and *B. subtilis* cells. They noted cytoplasmic membrane disruption across all strains upon the introduction of ZnO particles due to their adhesion to bacterial surfaces. The negative charges on cell surfaces are primarily due to lipoteichoic acid within the membrane and teichoic acid in the peptidoglycan layer. The electrostatic interactions attract positive charges from ZnO nanocrystals to the cell surface. Consequently, the variance in the electrostatic gradient leads to surface damage to the cells.<sup>36</sup>

On the other hand, the reason why bacteria could resist ZnO ions, might be due to that, bacteria have developed sophisticated mechanisms to regulate the concentration of meta ions within their cells; this is achieved through efflux and influx pump systems, ensuring stable internal environment, zinc ( $Zn^{2+}$ ) is a vital example of a metal ion that bacteria meticulously control.<sup>37</sup>

Several bacterial species, including *Staphylococci*, *Streptococci* and *E. coli*, possess genes dedicated to zinc transport; for example, in *S. aureus*, the ZntA and ZntR genes play a crucial role in zinc homeostasis; the ZntA protein, located in the cell membrane, acts as an efflux pump, actively removing excess zinc ions.<sup>38</sup> Meanwhile, the ZntR protein functions as an adjuster, adjusting the activity of the Znt operon (including ZntA) based on zinc availability.<sup>39</sup>

#### CONCLUSIONS

This study is concentrated on the formation and characterization of zinc oxide nanostructures using two methods: green and chemical precipitation. Various analytical techniques, such as UV–Vis spectrophotometry, FE-SEM, EDS, XRD and FTIR spectroscopy, were used to characterize the prepared ZnO-NPs. The findings show that capped and uncapped-ZnO are crystalline with a wurtzite structure, and

the crystalline size is 20.3 nm. No effect was observed on the morphology of ZnO after adding the extract. According to the calculated band gap, the quantum confinement effect becomes stronger after introducing the sesame seeds extract. Zinc oxide nanoparticles show an antibacterial effect against all the chosen bacteria, and *E. coli* exhibited an enormous sensitivity for ZnO-NPs.

### ИЗВОД

#### НАНОЧЕСТИЦЕ ЦИНК-ОКСИДА: ЕКСПЕРИМЕНТАЛНА СТУДИЈА О СИНТЕЗИ, КАРАКТЕРИЗАЦИЈИ И БИОЛОШКОЈ АКТИВНОСТИ

AULA M. AL HINDAWI<sup>1</sup>, ZAHRAA M. ABD AL-AAMA<sup>1</sup>, JUMAN KHALEEL AL-SABBAGH<sup>2</sup> и MOHAMMED AWAD<sup>3,4</sup>

<sup>1</sup>Department of Chemistry, College of Education for Pure Science, University of Kerbala, Karbala, Iraq,

<sup>2</sup>College of Veterinary Medicine, University of Kerbala, Karbala, Iraq, <sup>3</sup>School of Engineering, Samarkand International University of Technology, Samarkand, Uzbekistan и <sup>4</sup>Department of Chemical Engineering, Toronto Metropolitan University, Toronto, Canada

Честице цинк-оксида нановеличине су успешно синтетисане применом безбедног метода, коришћењем екстракта семена сусама као редукујућег агенса у току процеса формирања наноструктура ZnO, који преводи јоне цинка у Zn. Структурне и оптичке особине припремљених ZnO честица су испитане применом већег броја техника, као што су UV-Vis спектрофотометрија, скенирајућа електронска микроскопија са емисионим пољем (FE-SEM), спектроскопија X-зрака са расподелом енергије (EDS), дифракција X-зрака (XRD) и Фурије трансформишућа инфрацрвена спектроскопија (FTIR). Процењене енергетске разлике за ZnO наночестице настале у присуству и одсуству екстракта су биле 3,94 eV, односно 3,88 eV, сугеришући ефекат квантног ограничења. Добијене честице имају облик цвета и изгледају као мале сфере. Таус дијаграм је коришћен за процену енергетске разлике ZnO наночестица. Резултати су показали да ZnO наночестице испољавају бактерицидну активност спрам Грам-позитивне бактерије *Staphylococcus hominis*, као и спрам Грам-негативних бактерија *Proteus mirabilis*, *E. coli*, *Acinetobacter baumannii*, *Pseudomonas aeruginosa* и *Klebsiella pneumoniae*.

(Примљено 19. марта, ревидирано 22. априла, прихваћено 24. августа 2024)

### REFERENCES

1. L. R. Thurlow, V. C. Thomas, L. E. Hancock, *J. Bacteriol.* **191** (2009) 6203 (<https://doi.org/10.1128/JB.00592-09>)
2. T. J. Foster, *FEMS Microbiol. Rev.* **41** (2017) 430 (<https://doi.org/10.1093/femsre/fux007>)
3. M. Ozdal, S. Gurkok, *ADMET DMPK* **10** (2022) 115 (<https://doi.org/10.5599/admet.1172>)
4. R. D. Desiati, M. Taspika, E. Sugiarti, *Mater. Res. Express* **6** (2019) 95059 (<https://doi.org/10.1088/2053-1591/ab155c>)
5. D. Sahu, N. R. Panda, *Curr. Nanosci.* **17** (2021) 162 (<https://doi.org/10.2174/1573413716999200728175722>)
6. C. Silva, F. Bobillier, D. Canales, F. Antonella Sepúlveda, A. Cament, N. Amigo, L. M. Rivas, M. T. Ulloa, P. Reyes, J. A. Ortiz, T. Gómez, C. Loyo, P. A. Zapata, *Polymers (Basel)* **12** (2020) 2132 (<https://doi.org/10.3390/polym12092132>)
7. R. C. De Souza, L. U. Haberbeck, H. G. Riella, D. H. B. Ribeiro, B. A. M. Carciofi, *Braz. J. Chem. Eng.* **36** (2019) 885 (<https://doi.org/10.1590/0104-6632.20190362s20180027>)

8. S. Yang, C. Feng, D. Spence, A. M. A. A. Al Hindawi, E. Latimer, A. M. Ellis, C. Binns, D. Peddis, S. S. Dhesi, L. Zhang, Y. Zhang, K. N. Trohidou, M. Vasilakaki, N. Ntallis, I. MacLaren, F. M. F. De Groot, *Adv. Mater.* **29** (2017) 1604277  
(<https://doi.org/10.1002/adma.201604277>)
9. H. Yang, J. Zhang, Z. Li, J. Huang, J. Wu, Y. Zhang, H. Ge, Y. Zhao, *Nanomaterials* **13** (2023) 2033 (<https://doi.org/10.3390/nano13142033>)
10. C. Pushpalatha, J. Suresh, V. Gayathri, S. Sowmya, D. Augustine, A. Alamoudi, B. Zidane, N. H. Mohammad Albar, S. Patil, *Front. Bioeng. Biotechnol.* **10** (2022) 917990  
(<https://doi.org/10.3389/fbioe.2022.917990>)
11. T. A. Singh, J. Das, P. C. Sil, *Adv. Colloid Interface Sci.* **286** (2020) 102317  
(<https://doi.org/10.1016/j.cis.2020.102317>)
12. L. E. Román, J. Huachani, C. Uribe, J. L. Solís, M. M. Gómez, S. Costa, S. Costa, *Appl. Surf. Sci.* **469** (2019) 204 (<https://doi.org/10.1016/j.apsusc.2018.11.047>)
13. M. G. Kotresh, M. K. Patil, S. R. Inamdar, *Optik (Stuttgart)* **243** (2021) 167506  
(<https://doi.org/10.1016/j.ijleo.2021.167506>)
14. S. Arya, P. Mahajan, S. Mahajan, A. Khosla, R. Datt, V. Gupta, S.-J. Young, S. K. Oruganti, *ECS J. Solid State Sci. Technol.* **10** (2021) 23002 (<https://doi.org/10.1149/2162-8777/abe095>)
15. I. Ben Amor, H. Hemmami, S. E. Laouini, M. S. Mahboub, A. Barhoum, *Catalysts* **12** (2022) 1611 (<https://doi.org/10.3390/catal12121611>)
16. M. M. El-Faham, A. M. Mostafa, E. A. Mwafy, *J. Phys. Chem. Solids* **154** (2021) 110089  
(<https://doi.org/10.1016/j.jpcs.2021.110089>)
17. C. R. Mendes, G. Dilarri, C. F. Forsan, V. de M. R. Sapata, P. R. M. Lopes, P. B. de Moraes, R. N. Montagnolli, H. Ferreira, E. D. Bidoia, *Sci. Rep.* **12** (2022) 2658  
(<https://doi.org/10.1038/s41598-022-06657-y>)
18. M. I. Khan, S. Shah, S. Faisal, S. Gul, S. Khan, Abdullah, S. A. Shah, W. A. Shah, *Micromachines* **13** (2022) 1 (<https://doi.org/10.3390/mi13050668>)
19. M. Zare, K. Namratha, S. Alghamdi, Y. H. E. Mohammad, A. Hezam, M. Zare, Q. A. Drmosh, K. Byrappa, B. N. Chandrashekhar, S. Ramakrishna, X. Zhang, *Sci. Rep.* **9** (2019) 8303 (<https://doi.org/10.1038/s41598-019-44309-w>)
20. A. M. Al Hindawi, I. Joudah, S. Hamzah, Z. Tarek, *IOP Conf. Ser. Mater. Sci. Eng.* **571** (2019) 12069 (<https://doi.org/10.1088/1757-899X/571/1/012069>)
21. A. M. Al Hindawi, N. H. Obaid, I. Joudah, N. Shiltagh, K. Tahir, *Int. J. Pharm. Res.* **12** (2020) (<https://doi.org/10.31838/ijpr/2020.12.02.0150>)
22. A. Miri, M. Khatami, O. Ebrahimi, M. Sarani, *Green Chem. Lett. Rev.* **13** (2020) 27  
(<https://doi.org/10.1080/17518253.2020.1717005>)
23. L. Alsaba, M. Ashoush, S. Elsayed, A. Eid, A. Abdelghany, *Al-Azhar Bull. Sci.* **30** (2019) 1 (<https://doi.org/10.21608/absb.2019.86747>)
24. Z. Turki, A. Al Hindawi, N. Shiltagh, *NanoWorld J.* **08**  
(<https://doi.org/10.17756/nwj.2022-102>)
25. A. Abed, A. Al Hindawi, H. Alesary, *NanoWorld J.* **08**  
(<https://doi.org/10.17756/nwj.2022-103>)
26. P. Shunmuga Sundaram, T. Sangeetha, S. Rajakarthiham, R. Vijayalakshmi, A. Elangovan, G. Arivazhagan, *Phys., B* **595** (2020) 412342  
(<https://doi.org/10.1016/j.physb.2020.412342>)
27. W. Muhammad, N. Ullah, M. Haroon, B. H. Abbasi, *RSC Adv.* **9** (2019) 29541  
(<https://doi.org/10.1039/C9RA04424H>)

28. A. Q. Abed, A. M. Al Hindawi, H. F. Alesary, *AIP Conf. Proc.* **2830** (2023) 20001 (<https://doi.org/10.1063/5.0156826>)
29. Z. T. Turki, A. M. Al Hindawi, N. M. Shiltagh, *AIP Conf. Proc.* **2834** (2023) 30008 (<https://doi.org/10.1063/5.0161450>)
30. N. Jayarambabu, B. S. Kumari, K. V. Rao, Y. T. Prabhu, *Int. J. Curr. Eng. Technol.* **4** (2014) 3411 (<https://inpressco.com/wp-content/uploads/2014/09/Paper593411-3416.pdf>)
31. M. Hraja, A. Al Hindawi, N. Shiltagh, *J. Turkish Chem. Soc.* **11** (2011) 565 (<https://doi.org/10.18596/jotcsa.1356389>)
32. P. J. Kanu, *Amer. J. Biochem. Mol. Biol.* **1** (2012) 145 (<https://doi.org/10.3923/ajbmb.2011.145.157>)
33. S. Alamdari, M. Sasani Ghamsari, C. Lee, W. Han, H.-H. Park, M. J. Tafreshi, H. Afarideh, M. H. M. Ara, *Appl. Sci.* **10** (2020) 3620 (<https://doi.org/10.3390/app10103620>)
34. M. J. Klink, N. Laloo, A. Leudjo Taka, V. E. Pakade, M. E. Monapathi, J. S. Modise, *Molecules* **27** (2022) 3532 (<https://doi.org/10.3390/molecules27113532>)
35. B. Abebe, E. A. Zereffa, A. Tadesse, H. C. A. Murthy, *Nanoscale Res. Lett.* **15** (2020) 190 (<https://doi.org/10.1186/s11671-020-03418-6>)
36. N. B. Raj, N. T. PavithraGowda, O. S. Pooja, B. Purushotham, M. R. A. Kumar, S. K. Sukrutha, C. R. Ravikumar, H. P. Nagaswarupa, H. C. A. Murthy, S. B. Boppana, *J. Photochem. Photobiol.* **6** (2021) 100021 (<https://doi.org/10.1016/j.jphotobiol.2021.100021>)
37. J. K. Al-Sabbagh, A. Abd Al-Redha, M. A. Mohammad, *Ind. J. Public Health Res. Dev.* **11** (2020) 1123 (<https://www.researchgate.net/publication/345508208>)
38. C. C. Murdoch, E. P. Skaar, *Nat. Rev. Microbiol.* **20** (2022) 657 (<https://doi.org/10.1038/s41579-022-00745-6>)
39. B. Tartilán-Choya, C. Tejedor, R. Conde-Álvarez, P. María Muñoz, N. Vizcaíno, *Front. Vet. Sci.* **10** (2024) (<https://doi.org/10.3389/fvets.2023.1323500>).